Journal of Robotics and Control (JRC)
Volume 4, Issue 3, May 2023
ISSN: 2715-5072, DOI: 10.18196/jrc.v4i3.18225

A Novel Variable Stiffness Compound Extensor-Pneumatic Artificial Muscle (CE-PAM): Design and Mathematical Model

Wafaa Al-Mayahi [1]*, Hassanin Al-Fahaam [2]
[1, 2] Department of Computer Engineering, University of Basrah, Basrah, Iraq
Email: [1] engpg.wafaa.daraj@uobasrah.edu.iq, [2] hassanin.husein@uobasrah.edu.iq
*Corresponding Author

***Abstract*—Pneumatic artificial muscles (PAMs) have been exploited in robots utilized in various fields, including industry and medicine, due to their numerous advantages, such as their light weight; smooth, fast responses; and ability to generate significant force when fully extended. The actuator's stiffness is important in these applications, and extensor PAMs (EPAMs) have a lower stiffness when compared to contractor PAMs (CPAMs). Because of this, this research presents the compound extensor PAM (CE-PAM), which is a novel actuator that has higher stiffness and can alter its stiffness at a fixed length or maintain a fixed stiffness at a variable length. This makes it useful in applications such as surgery robots and wearable robots. The CE-PAM is created by inserting the CPAM into the EPAM. Then, a mathematical model is developed to calculate the output force using several mathematical equations that relate the force, actuator size, and applied pressure to each other. The force is also calculated experimentally, and when comparing the mathematical with the experimental results, the error percentage appears greater than 20%. So the mathematical model is enhanced by calculating the wasted energy consumed by the actuator before the start of the bladder's expansion, at which the force is zero because the pressure is consumed only for bladder expansion to touch the sleeve. The effect of the bladder's thickness is calculated to further enhance the model by calculating the volume of air entering the muscle rather than the total muscle volume. To illustrate the effect of thickness on the actuator, experiments are conducted on CPAMs made of the same bladder material but with different thicknesses. A balloon is used in the manufacture of the bladder. Because it is a lightweight, thin material with a low thickness, it requires very low pressure to expand.**

Keywords*—Soft Robot; Soft Actuator; Pneumatic Artificial Muscle (PAM); Modeling; Variable Stiffness.

I. INTRODUCTION

Pneumatic muscles are soft actuators that convert pneumatic energy into a pulling or pushing force [1]. The Bridgestone Company produced the first commercial version of the pneumatic artificial muscle (PAM) [2]. It is used to construct soft robots with several bendable joints and a high degree of freedom, rather than rigid robots with discrete fixed joints [3–7]. These robots provide safer interactions with humans when directly in contact with their bodies [8–12]. Pneumatic artificial muscle actuators are particularly useful in prosthetics and robotics inspired by organisms; they can be used as skeletal muscles' first-order hardware models [13, 14]. They are also widely utilized in limb rehabilitation robots [15–19] for people affected by strokes or other causes of weak limbs [20–24]. This is due to their functional resemblance to biological muscle in terms of contracting in response to activation and introducing compliance into the system [25–27]. The most important features of PAMs are summarized as follows:

- Lightweight [28, 29].
- Low-cost production components [30–32].
- A strength-to-weight ratio capable of producing high force under full pressure [33–36].
- Easily replaceable by separating the muscle and actuator tubing when damaged [2, 37].
- Flexible and capable of bending [20, 38].
- High degree of freedom [39].
- Built from soft materials.

Richard Gaylord invented the pneumatic muscle actuator [40, 41], but it was made popular by Joseph L. McKibben [42], so it was defined as the McKibben actuator [43–45]. The pneumatic actuator comprises three major components: a rubber tube covered in a braided sleeve, with appropriate plastic or metal fittings fitted to both ends of the tube [28, 46–49]. The tube and sleeve select the type of actuator by varying their length to produce either a contraction actuator that results in a pull force or an extension actuator that results in a push force [50–52]. Contractor PAMs (CPAMs) can produce higher forces than extensor PAMs (EPAMs) and are less prone to bending; thus, CPAMs are more widely used and are also referred to as contractile actuators [53–55]. The contraction or extension rate is determined by many parameters, including the inner bladder characteristics, the dimensions of the braided mesh, and the braided angle [56–59]. Furthermore, increasing the pressure in the contraction muscle causes the diameter to expand by up to 46%, which limits the contraction [60].

Carvalho et al. [28] developed and tested twelve pneumatic muscles made of different materials and at different sizes to find the most suitable ones for their application: the design and development of an elbow exoskeleton. Experiments have shown that muscles with higher tensile units decelerate less and handle loads better but have lower contraction and force characteristics. The same authors previously developed and tested four muscle

actuators with novel end fittings to show operational diversity; the new end fittings assisted in creating a lightweight, cost-effective PAM. The authors utilised different diameters to show how size affects the actuator's behaviour. They used styrene, which has a tensile modulus similar to skeletal muscle, to construct the PAMs. They also developed three mathematical models [61]. Koizumi et al. achieved a contraction rate of up to 37% by braiding the McKibben muscles together in the actuator, but this model achieved a lower contraction force [62].

Accurately controlling PAM-powered robots is a major challenge due to their nonlinear functioning [51, 63–65]. Thus, creating an accurate mathematical model of a PAM is a difficult task. The viscoelastic characteristics of the PAM's bladder, the mesh shell, and the compressibility of the air all contribute to nonlinearities, and the inner bladder causes hysteresis, so the performance varies depending on the circumstances [66–69]. Most mathematical models for analysing the force of a PAM's contraction use Chou's model [14], which ignores the expansion of the threads in the sleeve and the friction force between the sleeve and the bladder. Chou's model facilitates mathematical calculations because it is difficult to measure the force of the friction and the stretching of the threads. However, the model's accuracy decreases because of these factors' effects on muscle geometry, force, and consequence [41, 70].

Ensuring the robot is lightweight, highly flexible, and capable of achieving variable stiffness is the best way to make it more compatible with its required task and safer for human interactions. This is because a robot with variable stiffness can switch between resistance components and comply with the external force, and the increased stiffness of the robot makes positioning more accurate [54]. At the same time, it can be compliant when necessary for the task. Consequently, incorporating variable stiffness capability into continuum robots becomes important in robot design [65]. Therefore, many researchers are interested in achieving variable stiffness [71–74]. One method for this is to fill the muscles with high-mass coefficient liquids like water, but this increases the weight of these actuators' structures [75–77]. Most designs aiming to achieve variable stiffness depend on combining contractor and extensor muscles [54, 78, 79], where two actuators can oppose each other and thus control the stiffness. However, these designs require high pressure, which increases the risks associated with human–robot interactions [65]. The stiffness depends on the applied pressure, which the force also depends on. With an increase or decrease in pressure, the length of the actuator increases or decreases, and thus the expansion or contraction force and the stiffness increase. Therefore, the stiffness cannot be altered without altering the force or the actuator's length [80]. Because of this, Al-Fahaam's model [8] focused on independently changing the length and stiffness. This was achieved by constructing a CPAM that was proportionally longer than the EPAM and inserting it inside the EPAM, where a bidirectional muscle was designed based on the ratio of the length difference between the CPAM and EPAM. However, this resulted in only a 15% expansion.

This research contributed to soft robots by presenting the design of a novel variable stiffness actuator that could alter its stiffness at a fixed length and its length at a fixed stiffness, resulting in a 30% expansion. This actuator can be used to design various robots in contact with humans, such as surgical, wearable, and industrial robots. The variable stiffness actuator is regarded as the most promising mechanism for enhancing robots, with capabilities similar to those of a human joint. This paper can be divided into two sections. The first section describes the CE-PAM mathematical model for calculating the force of the actuator by calculating each of the bladder variables, sleeve variables, and pressure applied to the actuator, followed by enhancements to this model and practical experiments to demonstrate its validity. The second section describes the practical experiments carried out to achieve variable stiffness. Fig. 1. shows the research methodology and key steps.

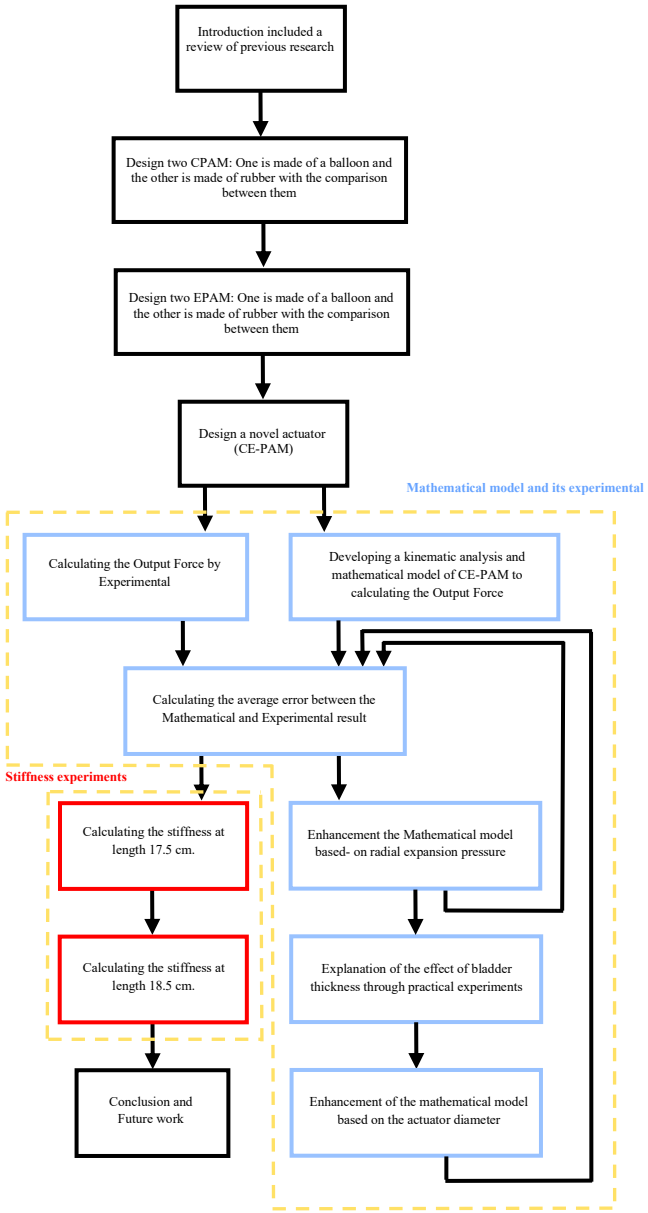

Fig. 1. Flow chart histogram of Research Methodology

II. CONTRACTION PNEUMATIC ARTIFICIAL MUSCLE

The contraction muscle is made up of an inner bladder and a braided sleeve of the same length and diameter. Also, there are two 3D-printed ends, one has a port for air to enter the muscle, and the other is closed. The angle formed by the sleeve threads is less than 54.7 degrees. If pressure is applied, it causes an expansion in a radial direction on the muscle, increasing the angle between the threads, which leads to an increase in diameter and a shortening of the length of the muscle, resulting in Pull force as shown in Fig. 2.

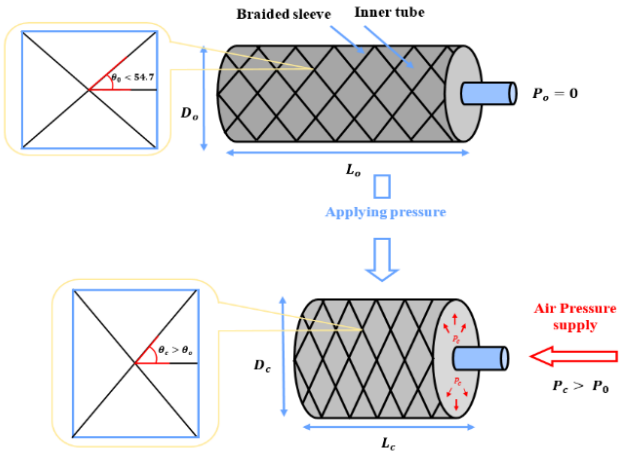

Fig. 2. The structure of the contraction muscle and its operation principle

Where L_0 and D_0 represent the length and diameter of the actuator at rest, respectively, and θ_0 for the angle formed between the single sleeve thread and the central axis which increases as applied pressure increases to θ_c, causing the length and diameter of the muscle to change to L_c and D_c, and P_c is the pressure applied to the contraction muscle.

Two contracting muscles were constructed, one of which was the inner bladder which is made of rubber tubes, while the other was made of a balloon of the same length and diameter (the length of the muscle is 19.5 cm and the diameter is 5 mm). Fig. 3. illustrates the contractor tube muscle and the contractor balloon muscle when the same pressure is applied to each of them at various degrees.

It was noticed that the balloon muscle can contract more than the tube muscle at the same pressure, with the length of the balloon muscle reaching 14.1 cm at a pressure of 250 kPa, while the length of the tube muscle reaches 16.1 cm at the same pressure, as shown in Fig. 4. Furthermore, the contraction potential of the balloon muscle is large at low pressures since it begins to contract relatively large from pressure at 50 kPa and contracts clearly with a small increase in pressure, while the tube muscle gives a small percentage of contraction at low pressures and begins to contract gradually with an increase in pressure. This difference is related to the tube resistivity as it is greater than the balloon resistivity.

The length of the tube muscle at its maximum contraction (occurring at 500 kPa pressure) was 14.3 cm, and the contraction ratio was 26.67%. which is less than that of the balloon (at 250 kPa pressure), with a contraction ratio of 27.69%. This difference is due to the fact that balloon muscle is made of thin material therefore it can contract at a good ratio at 250 kPa pressure.

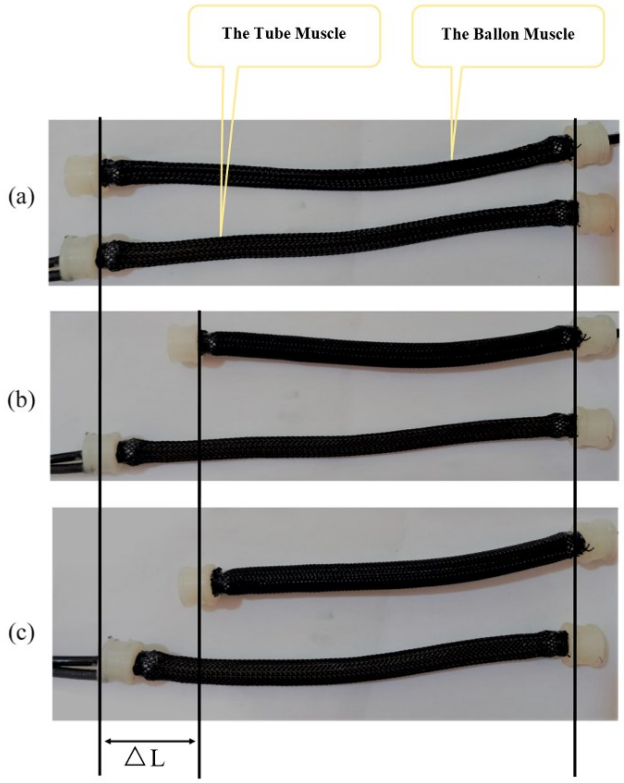

Fig. 3. The contraction tube muscle and the contraction balloon muscle at different pressures: (a) at pressure 0 kPa the two muscles at the same length. (b) at 150 kPa the balloon muscle contracts significantly while the tube muscle contracts only a little. (c) at 250 kPa The balloon muscle reaches its maximum contraction while the tube muscle contracts slightly more

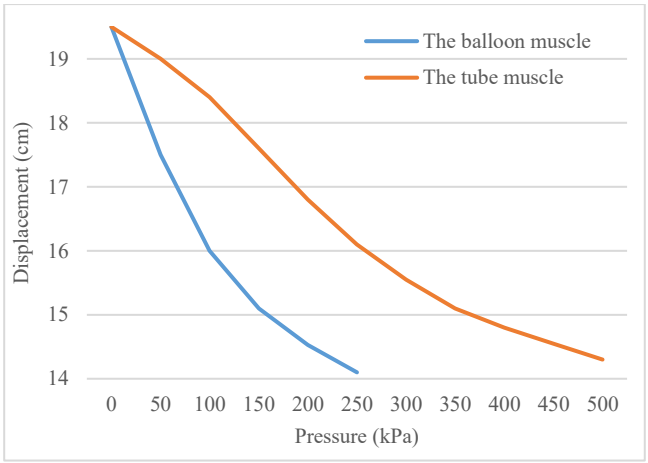

Fig. 4. The displacement difference between the contraction tube muscle and the contraction balloon muscle with increased applied pressure

To calculate the force and consequently the stiffness, the balloon contraction muscle was positioned vertically where the air-connected end is connected to a fixation plate and a load of various weights was attached to the other end as shown in Fig. 5. Four different pressures (100 kPa, 150 kPa, 200 kPa, and 250 kPa) were applied to the balloon muscle with several different weights for each pressure. The increase in length was recorded for each load. The stiffness is calculated mathematically by calculating the force for each load divided by the change in length and taking the average

of the results for these loads at a specific pressure, where the stiffness is the force divided by the displacement.

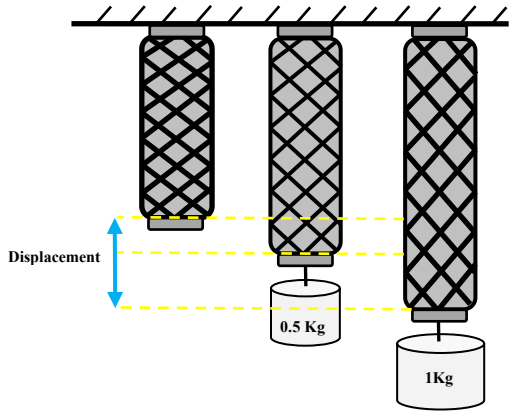

Fig. 5. Schematic description for stiffness measurement experiment

The stiffness increases proportionally with air pressure inside the muscle, reaching its maximum (727 N/m) at a pressure of 250 kPa. The results are shown in Fig. 6 and Fig. 7. which show that the force-displacement curves are approximately linear, also the balloon contraction muscle stiffness increases with increasing air pressure.

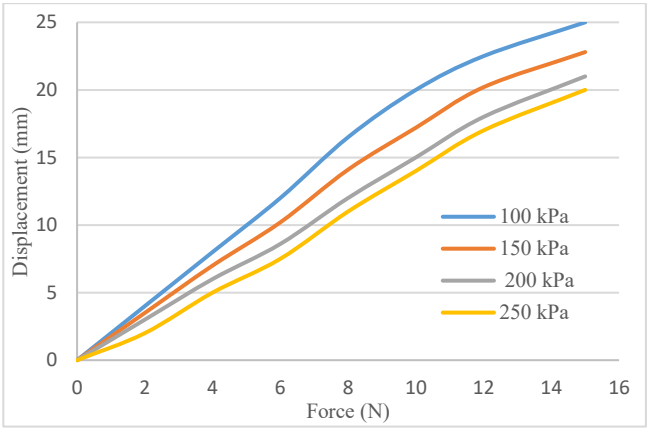

Fig. 6. The correlation between force and muscle displacement

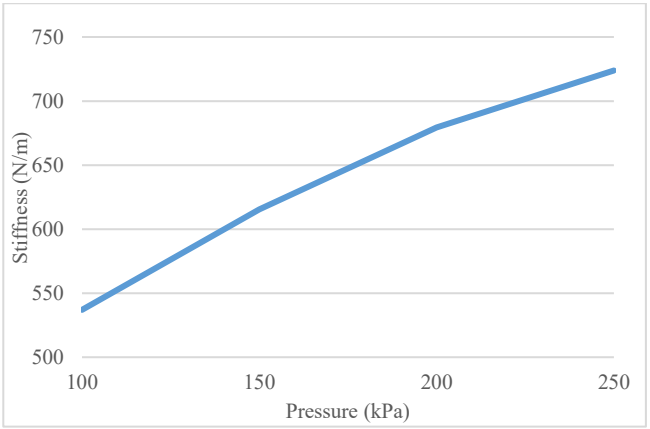

Fig. 7. The correlation between the pressure and the stiffness

III. Extensor Pneumatic Artificial Muscle

The extensor muscle is made up of an inner bladder and a braided sleeve that is longer than the bladder and is compressed axially to fit the bladder's length. As a result, the angle between the sleeve thread and the central axis is greater than 54.7 degrees. As in the contracting muscle, the two ends of the muscle are also closed with a 3D-printed cap. When the pressure was applied to the muscle, the angle decreases, causing the diameter to decrease and the length to increase, resulting in the push force as illustrated in Fig. 8.

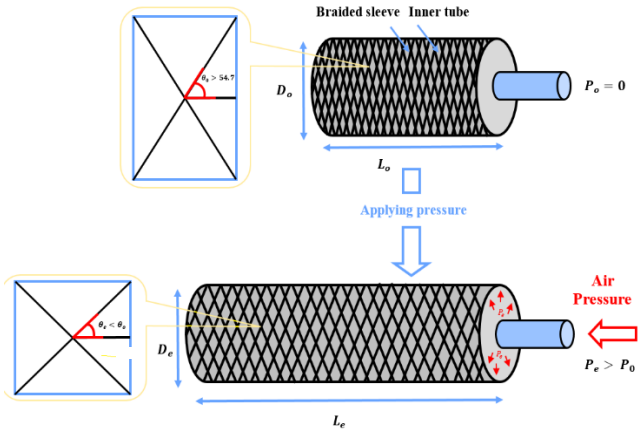

Fig. 8. The structure of the extensor muscle and its operation principle

Where, L_0 and D_0 represent the length and diameter of the actuator at rest, respectively, and θ_0 the angle formed between the single sleeve thread and the central axis which decrease as applied pressure increases to θ_e, causing the length and diameter of the muscle change to L_e and D_e, and P_e is the pressure applied to the contraction muscle.

Like in contracting muscles, two extensor muscles were structured, one from the balloon and the other from the tube, with the same length and diameter. However, the length of the inner bladder of the extensor muscle (15 cm) is shorter than that of the bladder of the previous contraction muscles and its diameter (10 mm) is double the diameter of the bladder of the contraction muscles, while the length of the braided sleeve of the extensor muscle (30 cm) is double of the length of its inner bladder, and its diameter same as the diameter of the bladder (10 mm).

Similar to the contracting muscle, the muscle made of a balloon expands at a much greater rate than the muscle made of a tube at low pressures, as shown in Fig. 9.

The balloon muscle extends significantly at 50 kPa (its length reaches 19.5 cm) in contrast to the tube muscle which has a shorter extension (15.5 cm). There was a linear correlation between pressure and extension in both muscles. However, at 150 kPa pressure, the balloon muscle's expansion was very small, while the tube muscle continued to gradually extend up to a pressure of 300 kPa. After this pressure, the increase in length becomes very small. The length of the tube muscle reached (23.3 cm) at a pressure of 500 kPa, and the extension ratio was 55.33%. The balloon muscle's pressure was stopped at 300 kPa because it had reached a high rate of expansion (23 cm) nearly reached the same rate of expansion as the tube muscle at 500 kPa, and the extension ratio of 53.33%. This is because it is made of a thin material that cannot withstand high pressures. Fig. 10. illustrates the expansion of both muscles with increasing pressures.

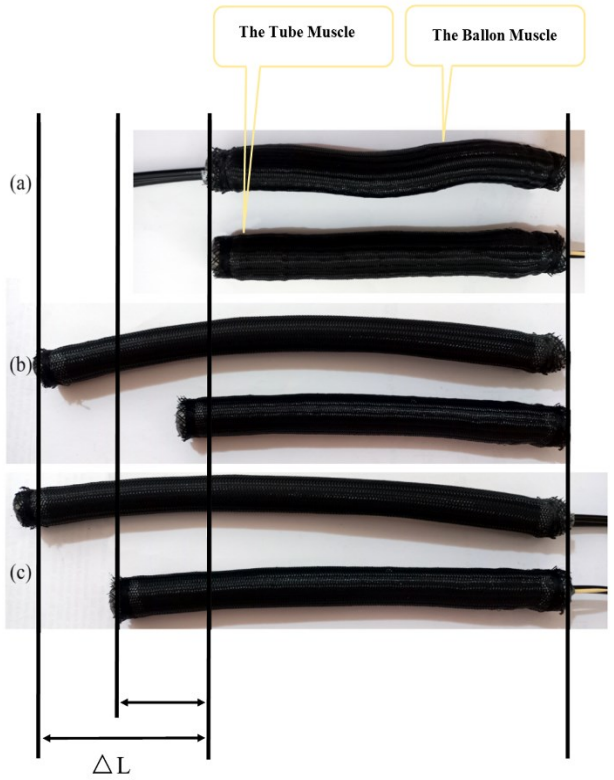

Fig. 9. The extensor tube muscle and the extensor balloon muscle at different pressures: (a) the two muscles at the same length at pressure 0 kPa, (b) the balloon muscle expands more than the tube muscle at 150 kPa, and (c) at 250 kPa The difference becomes less between the two muscles

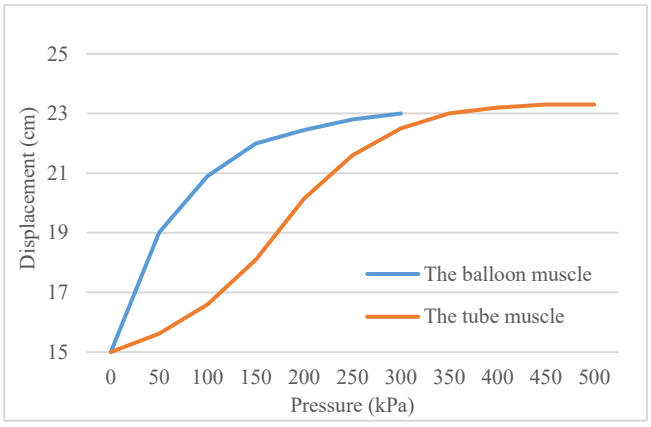

Fig. 10. The displacement difference between the extensor tube muscle and the extensor balloon muscle with increased applied pressure

To determine the stiffness, the extensor muscle experienced the same previous experiments in the contraction muscle and at the same pressures. The stiffness increases with the increase in air pressure inside the muscle, reaching its maximum (640 N/m) at a pressure of 250 kPa as Fig. 11. which shows that the force-displacement curves are approximately linear.

Fig. 12. shows the effect of applied pressure on muscle stiffness. As can be seen, the muscle's stiffness is low because of misalignment. Accordingly, a new muscle was developed by combining the extensor and contraction muscles to form the CE-PAM with greater stiffness, which will be discussed in more detail in the subsequent paragraphs.

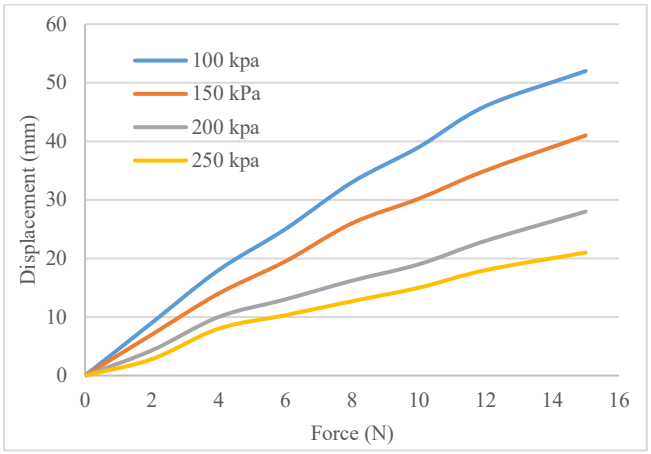

Fig. 11. The length of the extensor muscle increase with increased attached loads at different amounts of supplied pressure

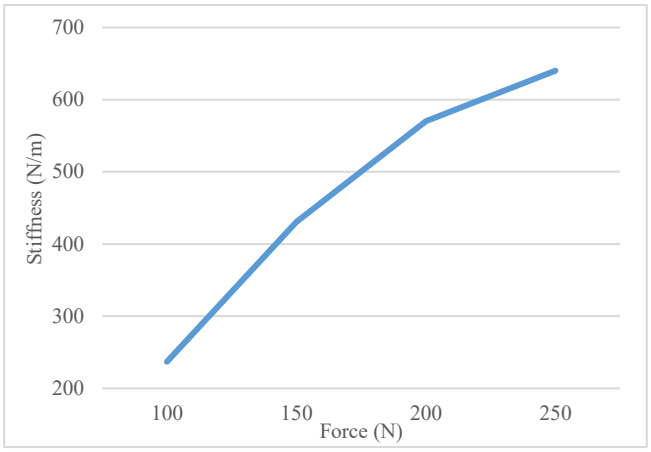

Fig. 12. The stiffness of the extensor muscle increases with increasing pressure applied

IV. Novel Compound Extensor-Pneumatic Artificial Muscle (CE-PAM)

The normal extensor muscle has little stiffness, as it is bent with increased air pressure inside it. Therefore, a novel extensor muscle was designed to overcome this limitation. The new muscle is characterized by:

- The compound extensor muscle has a higher stiffness than the extensor muscle.
- At fixed length, variable stiffness can be achieved.
- At variable lengths, constant stiffness can be achieved.
- With a few pressures, a good extension ratio can be achieved.

V. Design And Construction Of The Compound Extensor-Pneumatic Artificial Muscle

The CE-PAM is made up of a combination of a contraction muscle and an extensor muscle. The contraction muscle is positioned inside the extensor muscle. Both muscles are connected with the same 3D-printed ends. One end is blocked. The other end has two holes, one of which is central and connected to the contraction muscle so that compressed air can be applied to it. The other hole (side hole)

is supplied with compressed air and connected to the o extensor muscle can be seen in Fig. 13.

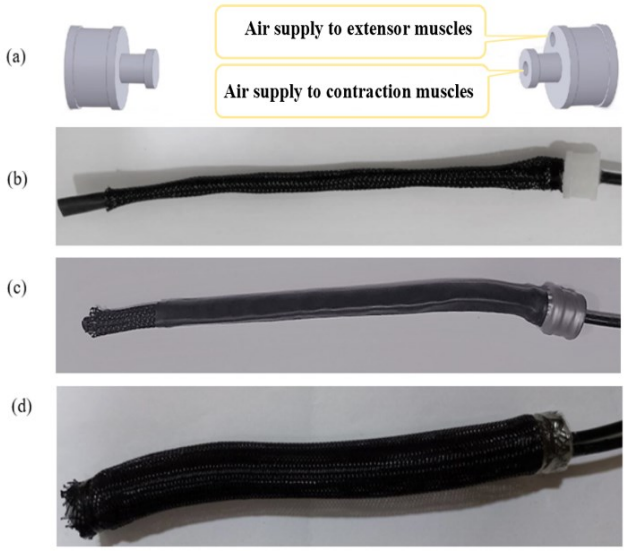

Fig. 13. Stages of CE-PAM manufacturing: (a) Design of the endcaps, (b) Connect the contraction muscle to one of the endcaps, (c) The contraction muscle is inserted into the bladder of the extensor muscle, and (d) The CE-PAM's final structure

The new compound muscle was formed using the same measurements applied to the two previous muscles. The bladder of the contraction muscle is connected to the small inner part of one of the end caps with adhesive material, then it was inserted with a braided sleeve of the same length as the bladder. The muscle was tied with thread and adhesive material for fixation, then it was inserted into the bladder of the extensor muscle. The length of the contraction muscle was 30% longer than that of the extensor muscle, therefore, the contraction muscle is compressed inside the bladder of the extensor, and the other end of each of the contraction muscle and the bladder of the extensor muscle was connected to the other end cap in the same way. Finally, the compound muscle was inserted with a braided sleeve which has the length of the bladder of the extensor muscle.

When the pressure was applied to the contraction muscle, it begins to contract until it reaches its maximum contraction rate, which was 30% of its initial length, at which the contractor muscle was as long as the extensor muscle (15 cm). With the reduction of pressure on the contraction muscle and increase pressure on the extensor muscle, the contractor muscle began to reduce contraction, which means a return to its initial length. On the other hand, the extensor muscle extended causing the compound muscle to extend until it reaches its maximum expansion rate (19.5 cm) at pressure 250 kPa, which is the initial length of the contraction muscle as the contracting muscle prevents it from more extension. The contraction muscle returned to its original length when the pressure inside it was 0 kPa.

VI. KINEMATIC ANALYSIS OF THE COMPOUND EXTENSOR-PNEUMATIC ARTIFICIAL MUSCLE

As previously mentioned in the contracting and extensor muscles, L and D represent the length and diameter of the muscle, respectively, and θ represents the angle formed by the single thread and the central axis, whereas b is the thread's length and n is the number of turns of the thread around the bladder. The general geometry of the muscle will be as shown in Fig. 14. assuming that the actuator's middle part is cylindrical.

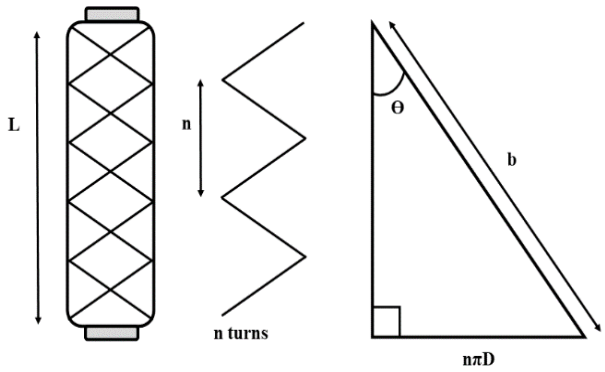

Fig. 14. The general geometry of PAM

The equation (1) and (2) can be used to calculate the length (L), width (D) based on Fig. 14.

$$L = b\ \cos\theta \tag{1}$$

$$D = \frac{b \sin\theta}{n\pi} \tag{2}$$

By an assumption that the volume of the muscle (V) is cylindrical in equation (3).

$$V = \frac{\pi D^2 L}{4} \tag{3}$$

The geometrical kinematics analysis of the compound muscle is illustrated in Fig. 15. where the contraction muscle is represented in red color and the extensor muscle in blue. To facilitate calculations, the analysis of the compound muscle is based on the assumption that there are no elastic forces within the bladders, and absence of friction forces between the braid's nylon threads, the contractor muscle and the extensor muscle's bladder, or between the braids and the bladders.

The CE-PAM is formed by using the same braid and bladder for both muscles, but in different sizes, as explained in the previous paragraphs. The contracting muscle has half the diameter of the extensor and is 30% longer in length. As the contraction muscle is longer than the extensor muscle, it is compressed within it.

The equation (4) and (5) expresses the relation between the contraction and extensor muscle lengths.

$$L_c = L_e + 0.3\ L_e \tag{4}$$

$$L_c = 1.3\ L_e, \quad L_e = \frac{1}{1.3} L_c \tag{5}$$

Where L_c is the contraction muscle's length and L_e is the extensor muscle's length.

As the length of the sleeve in the extensor is double that of the bladder, the relation between the length of the extensor's thread (b_e) and the length of the contractor's thread (b_c) will be as in equation (6).

$$2b_c = 1.3\ b_e, \quad b_e = \frac{2}{1.3} b_c \tag{6}$$

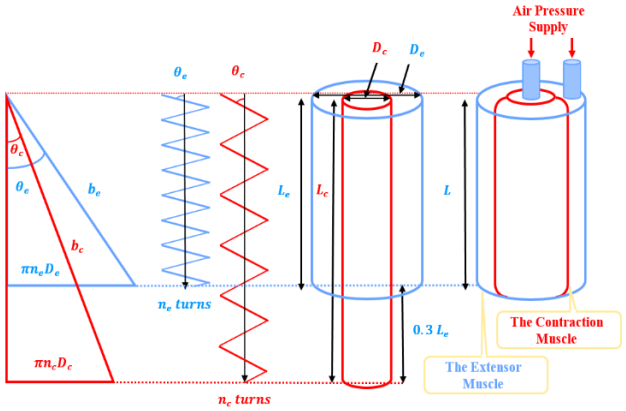

Fig. 15. Kinematics of the CE-PAM: (a) The general geometry of the contraction muscle and extensor muscle that make up the CE-PAM, (b) The braid angles and the number of turns of the two muscles, (c) Relation between muscles' lengths and, (c) The design of CE-PAM

The equation (7) can be used to calculate the number of turns of the extensor muscle from the contraction's turns and vice versa.

$$n_c = 1.3\, n_e, \;\; n_e = \frac{1}{1.3} n_c \tag{7}$$

Where n_c is the number of turns in the contractor's thread and n_e is the number of turns in the extensor's thread.

Similar to equation (1), (2), and (3), the geometric parameters for both the extensor and contraction muscles could be determined based on Fig. 14 and Fig. 15, which are obtained as in equation (8) to (10) for the contraction muscle, and equation (11) to (13) for the extensor muscle.

$$L_c = b_c \cos\theta_c \tag{8}$$

$$D_c = \frac{b_c \sin\theta_c}{\pi n_c} \tag{9}$$

$$V_c = \frac{\pi {D_c}^2 L_c}{4} \tag{10}$$

Where D_c, V_c, and θ_c are the diameter, volume, and angle formed by the single thread and the central axis of the contraction muscle, respectively.

$$L_e = b_e \cos\theta_e \tag{11}$$

$$D_e = \frac{b_e \sin\theta_e}{\pi n_e} \tag{12}$$

$$V_e = \frac{\pi {D_e}^2 L_e}{4} \tag{13}$$

Where D_e, V_e, and θ_e are the diameter, volume, and the angle formed by the single thread and the central axis of the extensor muscle, respectively.

VII. Modeling The Output Force Of The Compound Extensor-Pneumatic Artificial Muscle

Based on PAM's cylindrical shape, Chou et al. [29] derive the equation (14) mathematical model of the output force.

$$F = -P' \frac{dV}{dL} \tag{14}$$

Where P' denotes the relative PAM pressure.

As the contraction muscle is placed inside the extensor muscle, its relative pressure will be the difference between the contraction muscle's pressure (P_c) and the extensor muscle's pressure (P_e). So we get the equation (15).

$$P' = (P_c - P_e) \tag{15}$$

By substituting Eq. (15) by Eq. (14), it is possible to calculate the contractor force (F_c) as equation (16).

$$F_c = -(P_c - P_e)\frac{dV_c}{dL_c} \tag{16}$$

Eq. (16) is differentiated with respect to θ_c, can be seen in Eq. (17).

$$F_c = -(P_c - P_e)\frac{{dV_c}/{d\theta_c}}{{dL_c}/{d\theta_c}} \tag{17}$$

This means that the length and volume equations are differentiated with respect θ_c as shown in Eq. (18) and (19).

$$\frac{dV_c}{d\theta_c} = \frac{b_c^3 sin\theta_c}{4\pi n_c^2}(3\,cos^2\,\theta_c - 1) \tag{18}$$

$$\frac{dL_c}{d\theta_c} = -b_c sin\theta_c \tag{19}$$

As a result, the contractor force equation will be Eq. (20).

$$F_c = \frac{b_c^2 (P_c - P_e)}{4\pi n_c^2}(3\,cos^2\,\theta_c - 1) \tag{20}$$

It is worth mentioning that the volume of the muscle or cylinder refers to the volume of compressed air inside it. Thus, in the case of the extensor muscle, the volume of the cylindrical extensor muscle (V_s) is the difference between the extensor muscle's volume and the contraction muscle's volume. That is because the contraction muscle occupies a volume inside the extensor muscle. Consequently, the force in the extensor muscle (F_e) will be obtained equation (21) to (24).

$$F_e = P_e \frac{dV_s}{dL_e} = P_e \frac{dV_e - dV_c}{dL_e} = P_e \left(\frac{dV_e}{dL_e} - \frac{dV_c}{dL_e}\right) \tag{21}$$

By substituting Eq. (5) by Eq. (21), obtained equation (22).

$$F_e = P_e \left(\frac{dV_e}{dL_e} - 1.3\frac{dV_c}{dL_c}\right) \tag{22}$$

By differentiating $\frac{dV_e}{dL_e}$ with respect to θ_e, and substituting both Eq. (18) and (19) by Eq. (22), so obtained the equation (23).

$$F_e = P_e \left(1.3\,\frac{b_c^2(3\cos^2\theta_c - 1)}{4\pi n_c^2} - \frac{b_e^2(3\cos^2\theta_e - 1)}{4\pi n_e^2}\right) \tag{23}$$

The same Eq. (18) and Eq. (19) are obtained when deriving the volume and length of the extensor muscle with respect to θ_e only by replacing θ_c with θ_e and $b_c$with b_e.

By substituting Eq. (6) and (7) by Eq. (23), obtained equation (24).

$$F_e = \frac{b_e^2 P_e}{4\pi n_e^2}(0.325(3\cos^2\theta_c - 1) - (3\cos^2\theta_e - 1) \quad (24)$$

The resulting force of the CE-PAM muscle is the difference between the extensor muscle's force and the contraction muscle's force, because the force will be opposite where the extensor muscle produced a pushing force while the contraction muscle produced a pulling force. For the equation can be seen in Eq. (25).

$$F = (F_e - F_c) \quad (25)$$

VIII. Verification Of The Compound Extensor-Pneumatic Artificial Muscle Output Force Model By Experimentation

The extensor force of CE-PAM is measured by suspending it vertically; the air-connected end attaches to a mounting plate and the free end is attached to a load cell connected to the Arduino, which is connected to the computer to displays the muscle's extensor force as shown in Fig. 16. A regulator controls the air pressure that enters the muscle.

Fig. 16. Experimental setup of CE-PAM modeling: 1) CE-PAM, 2) the load cell, 3) the mounting plate, 4) Compressor for air pumping, 5) the air regulator, 6) Arduino, 7) Computer

In the beginning, the nominal length of the muscle is 15 cm, but with the increased pressure on contraction and the extensor muscles, the muscle extends. This causes a bending or lateral deformation of the muscle. Therefore, a rigid tube was used to surround the muscle to prevent such deformation as illustrated in Fig. 17.

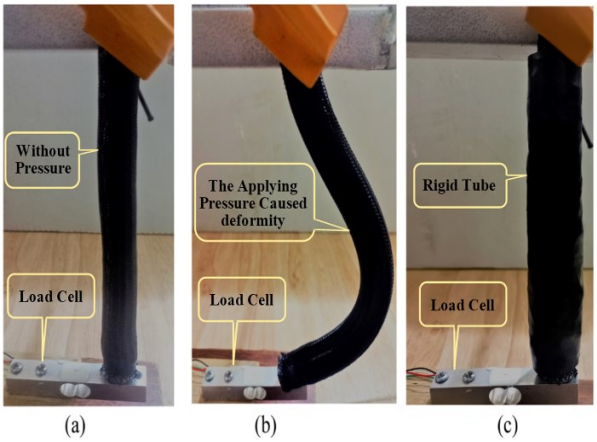

Fig. 17. The experimental operation to determine the CE-PAM's extension force: (a) CE-PAM at the beginning without pressure, (b) applying pressure to the CE-PAM causes a lateral bend or deformity, and (c) the CE-PAM surrounded by a rigid cylindrical tube to prevent deformity

Three experiments were performed to measure the extensor force of the CE-PAM. In each experiment, pressure on the contraction muscle was increased from 0 to 250 kPa, keeping the pressure on the extensor muscle fixed. The pressure was set at 100 kPa in the first experiment, 150 kPa in the second experiment, and 250 kPa in the third experiment. Fig. 18. displays the results of these experiments and their comparison to those obtained mathematically. It also illustrates the difference between experimental and theoretical results. For each of these three experiments, the average error percentages between the results are 21.56%, 20.24%, and 21.79%, respectively. The energy lost within the muscle is the cause of this error percentage.

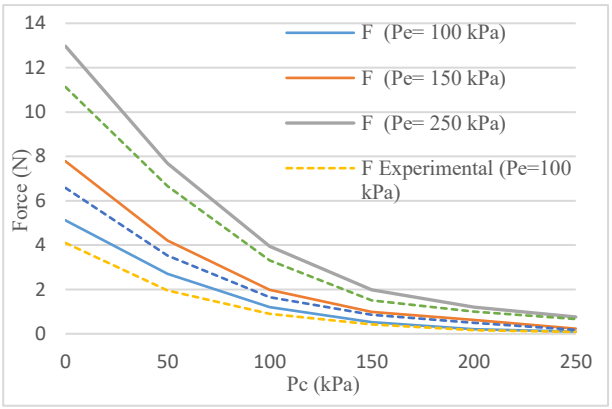

Fig. 18. Extensor force of the CE-PAM: experimental and mathematical results

IX. Enhancements To The Mathematical Model Based- On Radial Expansion Pressure

One of the factors associated with energy loss is that the bladder is not in contact with the sleeve. Thus, initial pressure renders the bladder to expand radially and contact with the sleeve. The output force would be equal to zero at this pressure. The muscle, then, contract or expand depending on the type of muscle [81], as depicted in Fig. 19.

The actual pressure (P_a) that renders the muscle to contract or expand is the muscle pressure (P) minus the pressure required to expand the bladder until its contact with the sleeve (P_r). For the equation can be seen in Eq. (26).

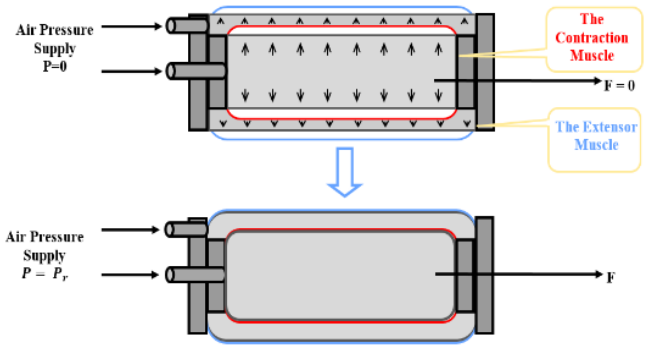

Fig. 19. The pressure required by the contraction and extensor muscles to expand the bladder

$$P_a = P - P_r \tag{26}$$

The actual pressure for contraction and extensor muscles was calculated using Tsagarakis and Caldwell's pressure model for radial expansion, which is expressed by the equation (27).

$$P_r = K_r(D_o - D_c \sin\theta) \tag{27}$$

Where D_o is the actual diameter of the muscle and K_r is the elasticity of the linearized radial actuator that obtains from the Eq. [82].

$$K_r = 2000 \frac{kPa}{m} \text{ for } D_c \sin\theta < \frac{D_o}{2}$$

$$K_r = 500 \frac{kPa}{m} \text{ for } D_c \sin\theta > \frac{D_o}{2}$$

The extensor muscle radial pressure is represented by the equation (28).

$$P_{re} = K_r(D_{oe} - D_e \sin\theta_e) \tag{28}$$

Where D_{oe} is the actual diameter of the extensor muscle. As such, the actual pressure of the extensor muscle will be obtained in Eq. (29).

$$P_{ae} = P_e - P_{re} \tag{29}$$

Substitution in Eq. (24) gives the extensor force Eq. (30).

$$\mathrm{F_e} = \frac{b_e^2 P_{ae}}{4\pi n_e^2}(0.325(3\cos^2\theta_c - 1) - (3\cos^2\theta_e - 1)) \tag{30}$$

Similarly, the actual pressure and the contraction force of the contraction muscle are calculated Eq. (31) and (32).

$$P_{ac} = P_c - P_{rc} \tag{31}$$

$$P_{rc} = K_r(D_{oc} - D_c \sin\theta_c) \tag{32}$$

Where D_{oc} is the actual diameter of the contraction muscle.

$$F_c = \frac{b_c^2\,(P_{ac} - P_{ae})}{4\pi n_c^2}(3\cos^2\theta_c - 1) \tag{33}$$

Fig. 20. shows the results obtained after this enhancement in comparison with the experimental result. A significant difference was found between these results and the previous results, as the average error percentages for each of the three experiments after the enhancement was 7.08 %, 6.23%, and 7.12%, respectively.

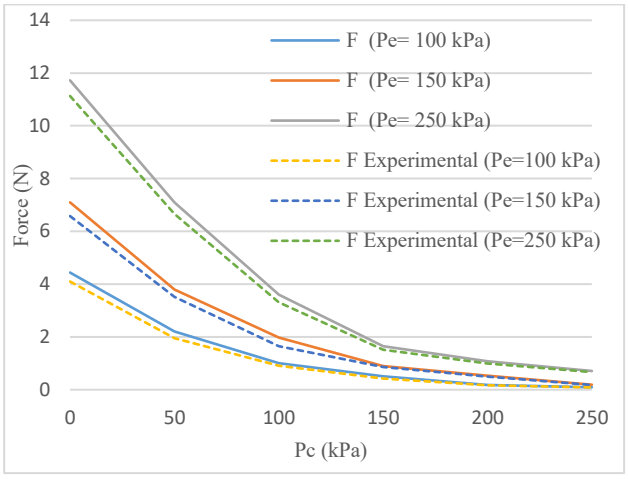

Fig. 20. The extensor force of the CE-PAM: the results of experimental and mathematical with P_r

X. The Effect Of Bladder Thickness On Muscle Contraction And Extension

The comparative experiments between the balloon and tube muscles showed the effect of thickness on the contraction and expansion ratio which can be attributed to the thickness difference between the balloon and tube (the balloon is made of thin material and has less thickness, while the tube is thicker). To better clarify the impact of thickness, three contraction muscles were made: the bladder of the first muscle is made of a tube with a thickness of 2 mm, the other muscle with a thickness of 1.5 mm, and the third muscle with a thickness of 1 mm, in addition to the balloon muscle, which is 1 mm thickness. The four muscles have the same diameter (5 mm) and length (19.5 cm).

When these muscles are pressed, the difference in contraction can be observed as illustrated in Fig. 21. The contraction ratio for the muscle with the largest thickness is 22.46%, 24.1% for the muscle with a thickness of 1.5, 26.67% for the muscle with the smallest thickness, and 27.69% for the balloon at a pressure of 500 kPa except for the balloon, which is at a pressure of 250 kPa. Fig. 22. show the difference in the muscles' length at these pressures. Similar to the effect of bladder thickness on contraction muscle, it also affects the extension of the extensor muscle.

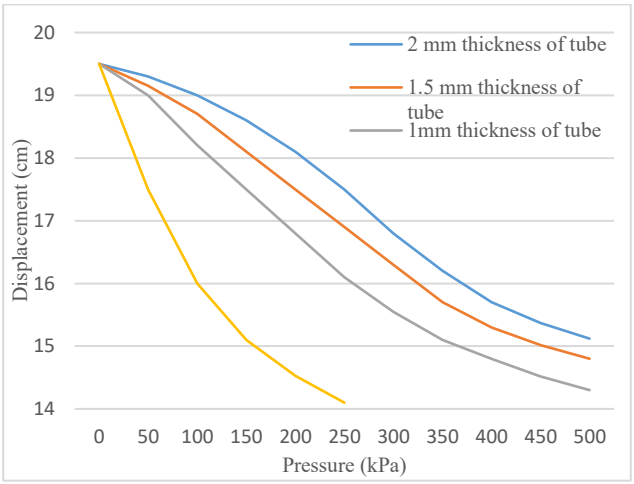

Fig. 21. The displacement differences between contraction muscles of different thicknesses

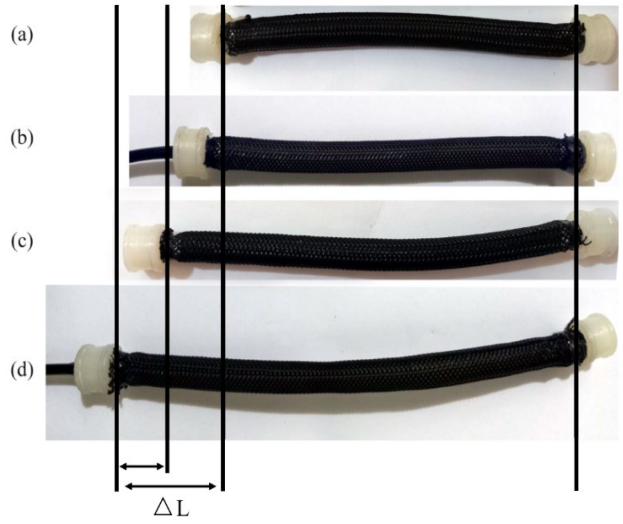

Fig. 22. Contraction muscles at 500 kPa pressure, and the balloon at 250 kPa pressure: (a) the balloon muscle with 1 mm thickness, (b) the tube muscle with 1 mm thickness, (c) the tube muscle with 1.5 mm thickness, and (d) the tube muscle with 2mm thickness

XI. Enhancements To The Mathematical Model Based- On Actuator Diameter

To reduce the percentage of error between the mathematical and experimental results, the thickness was calculated for both the bladder (t_b) and the sleeve (t_s).

The thickness of the muscle affects its diameter and, as a consequence, its volume. Hence, the actual muscle diameter (D_a) can be formulated as in the equation (34) and (35).

$$D_a = D_c - 2t_a \tag{34}$$

$$t_a = t_s + t_b \tag{35}$$

The actual extensor muscle diameter (D_{ae}) is obtained by the equation (36).

$$D_{ae} = D_e - 2t_a = \frac{b_e \sin\theta_e}{\pi n_e} - 2t_a \tag{36}$$

The actual extensor muscle volume (V_{ae}) is obtained by the equation (37).

$$V_{ae} = \frac{\pi {D_{ae}}^2 L_e}{4} = \frac{\pi b_e \cos\theta_e}{4}\left(\frac{b_e^2 \sin^2\theta_e}{\pi^2 n_e^2} - \frac{4\, t_a b_e \sin\theta_e}{\pi n_e} + 4t_a^2\right) \tag{37}$$

The extensor force can thus be calculated using Eq. (22) can be obtained the equation (38).

$$F_e = P_{ae}\left(\frac{dV_{ae}}{dL_e} - 1.3\frac{dV_c}{dL_c}\right) \tag{38}$$

Eq. (38) is differentiated with respect to θ_e and θ_c, so that the equations (39) to (41) is obtained.

$$F_e = P_{ae}\left(\frac{{dV_{ae}}/{d\theta_e}}{{dL_e}/{d\theta_e}} - 1.3\,\frac{{dV_c}/{d\theta_c}}{{dL_c}/{d\theta_c}}\right) \tag{39}$$

$$\frac{{dV_{ae}}/{d\theta_e}}{{dL_e}/{d\theta_e}} = \frac{b_e\, t_a}{n_e \sin\theta_e}(2\cos^2\theta_e - 1) - \frac{b_e^2}{4\pi n_e^2}(3\cos^2\theta_e - 1) + \pi t_a^2 \tag{40}$$

$$F_e = P_{ae}\left[\frac{b_e^2}{4\pi n_e^2}(0.325\,(3\cos^2\theta_c - 1) - (3\cos^2\theta_e - 1)) + t_a\left(\frac{b_e}{n_e \sin\theta_e}(2\cos^2\theta_e - 1) + \pi t_a\right)\right] \tag{41}$$

The thickness of the tube (t_b) and the braid sleeve (t_s) are equal in the extensor and contraction muscles. Obtained for the calculation as shown in the equation (42) and (43).

$$D_{ac} = D_c - 2t_a = \frac{b_c \sin\theta_c}{\pi n_c} - 2t_a \tag{42}$$

$$V_{ac} = \frac{\pi {D_{ac}}^2 L_c}{4} = \frac{\pi b_c \cos\theta_c}{4}\left(\frac{b_c^2 \sin^2\theta_c}{\pi^2 n_c^2} - \frac{4\, t_a b_c \sin\theta_c}{\pi n_c} + 4t_a^2\right) \tag{43}$$

The contraction force can thus be calculated using Eq. (44).

$$F_c = -(P_{ac} - P_{ae})\frac{dV_{ac}}{dL_c} \tag{44}$$

By differentiating with respect to θ_c, so obtained the equation (45).

$$F_c = -(P_{ac} - P_{ae})\left[\frac{b_c\, t_a}{n_c \sin\theta_c}(2\cos^2\theta_c - 1) - \frac{b_c^2}{4\pi n_c^2}(3\cos^2\theta_c - 1) + \pi t_a^2\right] \tag{45}$$

Fig. 23. illustrates the difference between mathematical and experimental thickness. The average error percentages for each of the three experiments after the enhancement was 5.132%, 4.54%, and 5.15%, respectively.

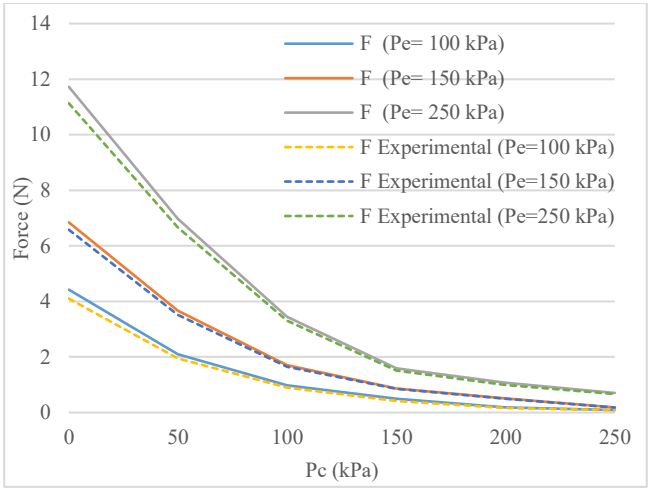

Fig. 23. Extensor force of the CE-PAM: experimental and mathematical results with t_a

XII. Stiffness Of The Compound Extensor-Pneumatic Artificial Muscle

The new CE-PAM can alter stiffness without changing its length or alter the length without changing the stiffness. This has been proved through experiments with varying pressures for both the contraction and extensor muscles that comprise the CE-PAM.

The muscle was hung vertically, as in previous stiffness experiments of the contraction and extensor muscles, but this

time the lower end remained free. The pressure was first applied to the extensor muscle until it reaches a length of 17.5 cm at a pressure of 50 kPa, then the pressure was increased for the contraction muscle to 75 kPa. However, the muscle length remains 17.5 cm. At that point, various loads were applied to the free end. The force of each load is calculated and the length measurement is taken manually to calculate the change in displacement at each load, the average of these results is calculated using the same previous methods for measuring stiffness, the stiffness is the force divided by the displacement

The experiment was repeated to obtain a different stiffness with a constant length, where a pressure of 75 kPa and 125 kPa was applied to the extensor and contraction muscles, respectively with a fixed muscle length of 17.5 cm. A higher stiffness was obtained this time than in the previous experiment. The experiment was repeated at pressures of Pe = 1 kPa and Pc = 175 kPa and, at Pe = 125 kPa and Pc = 250 kPa, and the displacement results were recorded to calculate the force and, consequently, the stiffness. The results are shown in Fig. 24. Different stiffness results (552.542N/m – 863.552N/m - 1060.361 N/m - 1387.296 N/m) were obtained as shown in Fig. 25.

It is possible to achieve fixed stiffness at a variable length by increasing the pressure on the extensor muscle to 75 kPa, to reach its length of 18.5 cm, then increasing the pressure on the contraction muscle to 1 kPa, and holding the muscle length at 18.5 cm. With a gradual increasing in pressure on both muscles (maintaining a length of 18.5 cm) and recording the stiffness values at a length of 17.5 cm as Fig. 26, it was found that when Pe = 125 kPa and Pc = 200 kPa the stiffness was (1084 N/m) and it was equal to the stiffness at length 17.5 cm when Pe =100 kPa and Pc = 175 kPa.

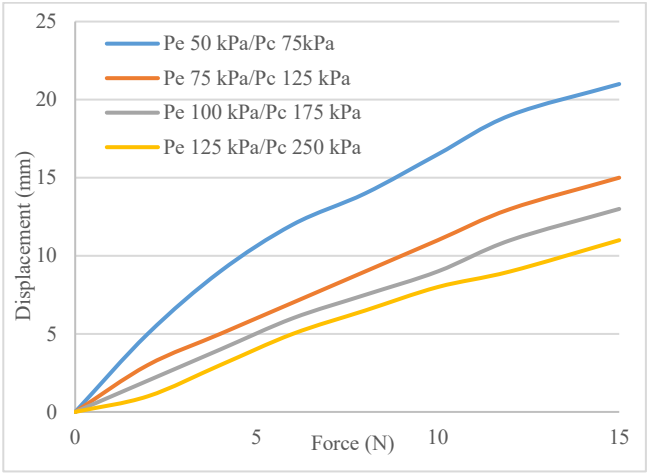

Fig. 24. The experimental results of the CE-PAM change in length with various attached loads at specific amounts of supplied pressure at a length of 17.5 cm

In Fig. 25 and Fig. 26 the stiffness is changed by controlling the pressure for both the EPAM and the CPAM. With the increase of pressure for each of these muscles, the stiffness will increase. The balloon was used in these experiments because it gave a good expansion under low pressures and did not need high pressures to expand significantly, but if the pressure is high, this leads to a burst of the balloon, that is, although the low pressure gives a good expansion, it limits the stiffness. The same experiments can be repeated to obtain higher stiffness by using different materials with higher resistance in muscle manufacture, such as rubber. It can withstand high pressures, which increases muscle stiffness.

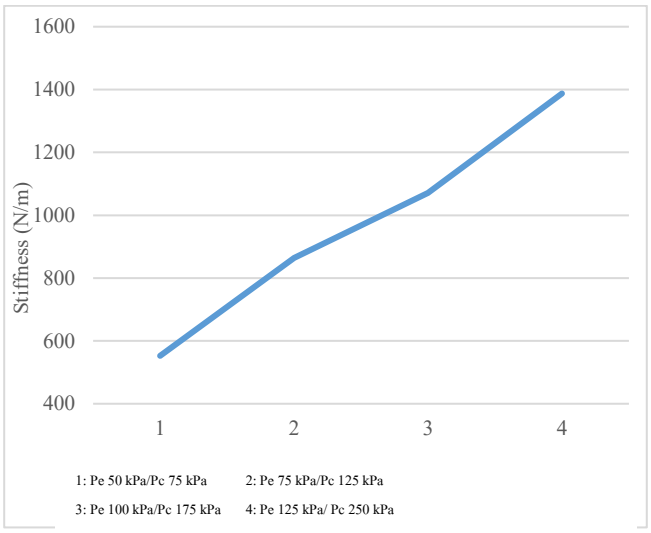

Fig. 25. CE-PAM stiffness at length 17.5 cm at different pressures

The muscle was manufactured and measurements were taken manually, this reduced the accuracy of the model. It can be manufactured in a factory to obtain better results.

It is worth noting that there is only one study to change the stiffness in this way, but it gave only a 15% expansion.

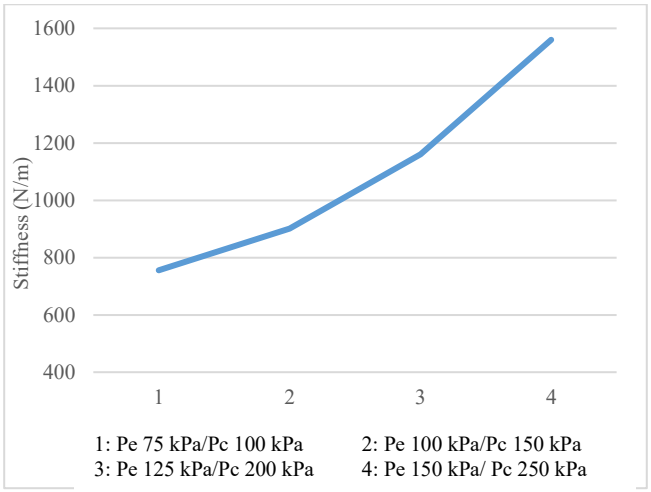

Fig. 26. CE-PAM stiffness at length 18.5 cm at different pressures

XIII. CONCLUSION

This paper described the design and development of the compound extensor PAM (CE-PAM), which achieved a 30% expansion capacity under low pressures. This muscle could change its stiffness at a specific length and maintain it at different lengths.

A mathematical model was developed to describe the CE-PAM's output force. To validate this model, three experiments were performed at pressures of 100 kPa, 150 kPa, and 250 kPa.

The average error between the experimental and mathematical models for these three experiments was 21.56%, 20.24%, and 21.79%, respectively. The mathematical model was improved by calculating the amount of wasted energy required to radially expand the bladder until it contacted the sleeve before the start of the expansion. The average error after this enhancement was 7.08%, 6.23%, and 7.12% at pressures of 100 kPa, 150 kPa, and 250 kPa, respectively. Additionally, the mathematical model was enhanced by calculating the bladder thickness after conducting experiments on muscles of various bladder thicknesses and demonstrating the effect of the thickness on the contraction ratio under the same pressure, the result shows that the difference in the contraction ratios reached approximately four percent between the largest and smallest thicknesses, the difference in the average error between the mathematical and experimental results of the three experiments reached 5.132%, 4.54%, and 5.15%. A balloon bladder was used because it could expand well under low pressures due to its low resistance, and it was thinner and lighter in weight than rubber tubes.

The most significant limitations of this work are that the muscle achieved only 30% extension and was manufactured manually, which reduced manufacturing accuracy. Additionally, although building the muscle from a balloon was less costly and lighter in weight, it caused misalignment, and friction was not reduced.

In future work, the model can be enhanced to reduce the error between the mathematical and experimental results by calculating the friction between the bladder and the sleeve and the friction between the sleeve threads. The model can also be applied to muscles of various sizes. This type of muscle will have useful applications in, for example, rehabilitation robots.

REFERENCES

[1] H. Al-Fahaam, S. Davis, and S. Nefti-Meziani, "Wrist rehabilitation exoskeleton robot based on pneumatic soft actuators," in *2016 International Conference for Students on Applied Engineering (ICSAE)*, pp. 491-496, 2016, doi: 10.1109/ICSAE.2016.7810241.

[2] B. Kalita, A. Leonessa, and S. K. Dwivedy, "A review on the development of pneumatic artificial muscle actuators: Force model and application," in *Actuators*, vol. 11, no. 10, p. 288, 2022, doi: 10.3390/act11100288.

[3] A. Alipour, M. Mahjoob, and A. Nazarian, "A New 4-DOF Robot for Rehabilitation of Knee and Ankle-Foot Complex: Simulation and Experiment," *Journal of Robotics and Control (JRC)*, vol. 3, no. 4, pp. 483-495, 2022.

[4] A. H. Noviyanto, L. D. Septilianingtyas, and D. Rahmawati, "Design of a Continuous Passive Motion (CPM) Machine for Wrist Joint Therapy," *Journal of Robotics and Control (JRC)*, vol. 2, no. 4, pp. 311-315, 2021, doi: 10.18196/jrc.2498.

[5] H. Q. T. Ngo and M. H. Nguyen, "Enhancement of the Tracking Performance for Robot Manipulator by Using the Feed-forward Scheme and Reasonable Switching Mechanism," *Journal of Robotics and Control (JRC)*, vol. 3, no. 3, pp. 328-337, 2022, doi: 10.18196/jrc.v3i3.14585.

[6] R. Kobayashi, H. Nabae, and K. Suzumori, "Large Torsion Thin Artificial Muscles Tensegrity Structure for Twist Manipulation," *IEEE Robotics and Automation Letters*, vol. 8, no. 3, pp. 1207-1214, 2023, doi: 10.1109/LRA.2023.3236889.

[7] Q. Ai, D. Ke, J. Zuo, W. Meng, Q. Liu, Z. Zhang, and S. Q. Xie, "High-order model-free adaptive iterative learning control of pneumatic artificial muscle with enhanced convergence," *IEEE Transactions on Industrial Electronics*, vol. 67, no. 11, pp. 9548-9559, 2019, doi: 10.1109/TIE.2019.2952810.

[8] H. Al-Fahaam, S. Nefti-Meziani, T. Theodoridis, and S. Davis, "The design and mathematical model of a novel variable stiffness extensor-contractor pneumatic artificial muscle," *Soft robotics*, vol. 5, no. 5, pp. 576-591, 2018, doi: 10.1089/soro.2018.0010.

[9] A. Al-Ibadi, S. Nefti-Meziani, and S. Davis, "Novel models for the extension pneumatic muscle actuator performances," in *2017 23rd international conference on automation and computing (ICAC)*, pp. 1-6, 2017, doi: 10.23919/IConAC.2017.8081973.

[10] S. Yeem, J. Heo, H. Kim, and Y. Kwon, "Technical analysis of exoskeleton robot," *World Journal of Engineering and Technology*, vol. 7, no. 1, pp. 68-79, 2018, doi: 10.4236/wjet.2019.71004.

[11] W. Najmuddin and M. Mustaffa, "A study on contraction of pneumatic artificial muscle (PAM) for load-lifting," in *Journal of Physics: Conference Series*, vol. 908, no. 1, p. 012036, 2017, doi: 10.1088/1742-6596/908/1/012036.

[12] A. U. Nisa, S. Samo, R. A. Nizamani, A. Irfan, Z. Anjum, and L. Kumar, "Design and Implementation of Force Sensation and Feedback Systems for Telepresence Robotic Arm," *Journal of Robotics and Control (JRC)*, vol. 3, no. 5, pp. 710-715, 2022, doi: 10.18196/jrc.v3i5.15959.

[13] X. Li, K. Sun, C. Guo, T. Liu, and H. Liu, "Enhanced static modeling of commercial pneumatic artificial muscles," *Assembly Automation*, vol. 40, no. 3, pp. 407-417, 2020, doi: 10.1108/AA-04-2019-0060.

[14] C.-P. Chou and B. Hannaford, "Measurement and modeling of McKibben pneumatic artificial muscles," *IEEE Transactions on robotics and automation*, vol. 12, no. 1, pp. 90-102, 1996, doi: 10.1109/70.481753.

[15] B. Chen, H. Ma, L.-Y. Qin, F. Gao, K.-M. Chan, S.-W. Law, L. Qin, and W.-H. Liao, "Recent developments and challenges of lower extremity exoskeletons," *Journal of Orthopaedic Translation*, vol. 5, pp. 26-37, 2016, doi: 10.1016/j.jot.2015.09.007.

[16] X. Chen, S. Zhang, K. Cao, C. Wei, W. Zhao, and J. Yao, "Development of a Wearable Upper Limb Rehabilitation Robot Based on Reinforced Soft Pneumatic Actuators," *Chinese Journal of Mechanical Engineering*, vol. 35, no. 1, p. 83, 2022, doi: 10.1186/s10033-022-00749-6.

[17] S. Biggar and W. Yao, "Design and evaluation of a soft and wearable robotic glove for hand rehabilitation," *IEEE Transactions on Neural Systems and Rehabilitation Engineering*, vol. 24, no. 10, pp. 1071-1080, 2016, doi: 10.1109/TNSRE.2016.2521544.

[18] B. Radder, G. B. Prange-Lasonder, A. I. Kottink, J. Holmberg, K. Sletta, M. van Dijk, T. Meyer, A. Melendez-Calderon, J. H. Buurke, and J. S. Rietman, "Home rehabilitation supported by a wearable soft-robotic device for improving hand function in older adults: A pilot randomized controlled trial," *PloS one*, vol. 14, no. 8, p. e0220544, 2019, doi: 10.1371/journal.pone.0220544.

[19] J. Zhong, D. He, C. Zhao, Y. Zhu, and Q. Zhang, "An rehabilitation robot driven by pneumatic artificial muscles," *Journal of Mechanics in Medicine and Biology*, vol. 20, no. 9, p. 2040008, 2020, doi: 10.1142/S0219519420400084.

[20] G. Gregov, S. Pincin, A. Šoljić, and E. Kamenar, "Position Control of a Cost-Effective Bellow Pneumatic Actuator Using an LQR Approach," in *Actuators*, vol. 12, no. 2, p. 73, 2023, doi: 10.3390/act12020073.

[21] X. Zhu and B. He, "Underactuated rehabilitation robotics for hand function," *Journal of Robotics and Control (JRC)*, vol. 2, no. 5, pp. 337-341, 2021, doi: 10.18196/jrc.25103.

[22] N. S. Shalal and W. S. Aboud, "Smart robotic exoskeleton: A 3-dof for wrist-forearm rehabilitation," *Journal of Robotics and Control (JRC)*, vol. 2, no. 6, pp. 476-483, 2021, doi: 10.18196/jrc.26125.

[23] L. Bai, "A Sensor Based Assessment Monitoring System for Patients with Neurological Disabilities," *Journal of Robotics and Control (JRC)*, vol. 2, no. 6, pp. 489-495, 2021, doi: 10.18196/jrc.26127.

[24] N. A. Alawad, A. J. Humaidi, and A. S. Alaraji, "Observer Sliding Mode Control Design for lower Exoskeleton system: Rehabilitation Case," *Journal of Robotics and Control (JRC)*, vol. 3, no. 4, pp. 476-482, 2022, doi: 10.18196/jrc.v3i4.15239.

[25] D. Rus and M. T. Tolley, "Design, fabrication and control of soft robots," *Nature*, vol. 521, no. 7553, pp. 467–475, May. 2015, doi: 10.1038/nature14543.

[26] M. J. Bennington, T. Wang, J. Yin, S. Bergbreiter, C. Majidi, and V. A. Webster-Wood, "Design and Characterization of Viscoelastic McKibben Actuators with Tunable Force-Velocity Curves," *2023 IEEE International Conference on Soft Robotics (RoboSoft)*, pp. 1-7, 2023, doi: 10.1109/RoboSoft55895.2023.10122014.

[27] T. Triwiyanto, W. Caesarendra, V. Abdullayev, A. A. Ahmed, and H. Herianto, "Single Lead EMG signal to Control an Upper Limb

Exoskeleton Using Embedded Machine Learning on Raspberry Pi," *Journal of Robotics and Control (JRC)*, vol. 4, no. 1, pp. 35-45, 2023, doi: 10.18196/jrc.v4i1.17364.

[28] A. D. D. R. Carvalho, N. Karanth, and V. Desai, "Characterization of pneumatic muscle actuators and their implementation on an elbow exoskeleton with a novel hinge design," *Sensors and Actuators Reports*, vol. 4, p. 100109, 2022, doi: 10.1016/j.snr.2022.100109.

[29] N. D. Naclerio and E. W. Hawkes, "Simple, low-hysteresis, foldable, fabric pneumatic artificial muscle," *IEEE Robotics and Automation Letters*, vol. 5, no. 2, pp. 3406-3413, 2020, doi: 10.1109/LRA.2020.2976309.

[30] L. Hines, K. Petersen, G. Z. Lum, and M. Sitti, "Soft actuators for small-scale robotics," *Advanced materials*, vol. 29, no. 13, p. 1603483, 2017, doi: 10.1002/adma.201603483.

[31] B. Gorissen, D. Reynaerts, S. Konishi, K. Yoshida, J. W. Kim, and M. De Volder, "Elastic inflatable actuators for soft robotic applications," *Advanced Materials*, vol. 29, no. 43, p. 1604977, 2017, doi: 10.1002/adma.201604977.

[32] F. Daerden and D. Lefeber, "Pneumatic artificial muscles: actuators for robotics and automation," *European Journal of Mechanical and Enviromental Engineering*, vol. 47, no. 1, pp. 11-22, 2002.

[33] G. K. Klute and B. Hannaford, "Accounting for elastic energy storage in McKibben artificial muscle actuators," *J. Dyn. Sys. Meas. Control*, vol. 122, no. 2, pp. 386-388, 2000, doi: 10.1115/1.482478.

[34] H. Majidi Fard Vatan, S. Nefti-Meziani, S. Davis, Z. Saffari, and H. El-Hussieny, "A review: A comprehensive review of soft and rigid wearable rehabilitation and assistive devices with a focus on the shoulder joint," *Journal of Intelligent & Robotic Systems*, vol. 102, pp. 1-24, 2021, doi: 10.1007/s10846-021-01353-x.

[35] Q. Xie, T. Wang, S. Yao, Z. Zhu, N. Tan, and S. Zhu, "Design and modeling of a hydraulic soft actuator with three degrees of freedom," *Smart Materials and Structures*, vol. 29, no. 12, p. 125017, 2020, doi: 10.1088/1361-665X/abc26e.

[36] X. Liu, J. Zhang, F. Xu, T. Wang, and L. Zhao, "Design and modelling of multi-DOF manipulator driven by hysteresis-attenuated pneumatic artificial muscles," *IEEE Robotics and Automation Letters*, vol. 7, no. 3, pp. 6447-6454, 2022, doi: 10.1109/LRA.2022.3172984.

[37] D. U. Rijalusalam and I. Iswanto, "Implementation kinematics modeling and odometry of four omni wheel mobile robot on the trajectory planning and motion control based microcontroller," *Journal of Robotics and Control (JRC)*, vol. 2, no. 5, pp. 448-455, 2021, doi: 10.18196/jrc.25121.

[38] A.-R. Ziad, M. Al-Ibadi, and A. Al-Ibadi, "Design and Implementation of a Multiple DoF Soft Robot Arm Using Exestensor Muscles," in *2022 9th International Conference on Electrical and Electronics Engineering (ICEEE)*, pp. 170-174, 2022, doi: 10.1109/ICEEE55327.2022.9772525.

[39] A. Al-Ibadi, "The Design and Implementation of a Single-Actuator Soft Robot Arm for Lower Back Pain Reduction," *The 3rd Scientific Conference of Electrical and Electronic Engineering Researches (SCEEER)*, 2020, doi: 10.37917/ijeee.sceeer.3rd.4.

[40] R. H. Gaylord, "Fluid actuated motor system and stroking device," ed: Google Patents, 1958.

[41] J. M. Chambers and N. M. Wereley, "Analysis of Pneumatic Artificial Muscles and the Inelastic Braid Assumption," in *Actuators*, vol. 11, no. 8, p. 219, 2022, doi: 10.3390/act11080219 .

[42] K. Ashwin and A. Ghosal, "A survey on static modeling of miniaturized pneumatic artificial muscles with new model and experimental results," *Applied Mechanics Reviews*, vol. 70, no. 4, 2018, doi: 10.1115/1.4041660.

[43] J. Zhang, J. Sheng, C. T. O'Neill, C. J. Walsh, R. J. Wood, J.-H. Ryu, J. P. Desai, and M. C. Yip, "Robotic artificial muscles: Current progress and future perspectives," *IEEE transactions on robotics*, vol. 35, no. 3, pp. 761-781, 2019, doi: 10.1109/TRO.2019.2894371.

[44] C. Zhang, P. Zhu, Y. Lin, W. Tang, Z. Jiao, H. Yang, and J. Zou, "Fluid-driven artificial muscles: bio-design, manufacturing, sensing, control, and applications," *Bio-Design and Manufacturing*, vol. 4, pp. 123-145, 2021, doi: 10.1007/s42242-020-00099-z.

[45] D. Gong and J. Yu, "Design and Control of the McKibben Artificial Muscles Actuated Humanoid Manipulator," in *Rehabilitation of the Human Bone-Muscle System: IntechOpen*, 2022, doi: 10.5772/intechopen.101761.

[46] M. S. Xavier *et al*., "Soft pneumatic actuators: A review of design, fabrication, modeling, sensing, control and applications," *IEEE Access*, vol. 10, no. 21779953, 2022, doi: 10.1109/ACCESS.2022.3179589.

[47] Ž. Šitum, S. Herceg, N. Bolf, and Ž. Ujević Andrijić, "Design, Construction and Control of a Manipulator Driven by Pneumatic Artificial Muscles," *Sensors*, vol. 23, no. 2, p. 776, 2023, doi: 10.3390/s23020776.

[48] B. Jamil, H. Rodrigue, and Y. Choi, "Design of a novel sensing method for a pneumatic artificial muscle actuator-driven 2-Degrees of freedom parallel joint," *Soft Robotics*, vol. 10, no. 1, pp. 187-196, 2023, doi: 10.1089/soro.2021.0097.

[49] A. Aliseichik *et al*., "Artificial Muscles," *Journal of Computer and Systems Sciences International*, vol. 61, no. 2, pp. 270-293, 2022, doi: 10.1134/S1064230722010026.

[50] W. Liu and C. Rahn, "Fiber-reinforced membrane models of McKibben actuators," *J. Appl. Mech*., vol. 70, no. 6, pp. 853-859, 2003, doi: 10.1115/1.1630812.

[51] J. Zuo, Q. Liu, W. Meng, Q. Ai, and S. Q. Xie, "Enhanced compensation control of pneumatic muscle actuator with high-order modified dynamic model," *ISA transactions*, vol. 132, pp. 444-461, 2023, doi: 10.1016/j.isatra.2022.06.012.

[52] S. Zhong, Z. Gai, Y. Yang, Y. Zhao, Y. Qi, Y. Yang, and Y. Peng, "A contraction length feedback method for the McKibben pneumatic artificial muscle," *Sensors and Actuators A: Physical*, vol. 334, p. 113321, 2022, doi: 10.1016/j.sna.2021.113321.

[53] S. Udhayakumar, R. Bharath, N. Kowshik Santhakumar, and B. Mohamed Samsudeen Soofi, "Review on Applications of Pneumatic Air Muscle," in *Advances in Forming, Machining and Automation: Select Proceedings of AIMTDR 2021*, pp. 655-666, 2022, doi: 10.1007/978-981-19-3866-5_52.

[54] L. Hao, C. Xiang, M. E. Giannaccini, H. Cheng, Y. Zhang, S. Nefti-Meziani, and S. Davis, "Design and control of a novel variable stiffness soft arm," *Advanced Robotics*, vol. 32, no. 11, pp. 605-622, 2018, doi: 10.1080/01691864.2018.1476179.

[55] D. Dragone, L. Randazzini, A. Capace, F. Nesci, C. Cosentino, F. Amato, E. De Momi, R. Colao, L. Masia, and A. Merola, "Design, Computational Modelling and Experimental Characterization of Bistable Hybrid Soft Actuators for a Controllable-Compliance Joint of an Exoskeleton Rehabilitation Robot," in *Actuators*, vol. 11, no. 2, p. 32, 2022, doi: 10.3390/act11020032 .

[56] A. Al-Ibadi, S. Nefti-Meziani, and S. Davis, "Efficient structure-based models for the McKibben contraction pneumatic muscle actuator: The full description of the behaviour of the contraction PMA," in *Actuators*, vol. 6, no. 4, p. 32, 2017, doi: 10.3390/act6040032.

[57] E. G. Hocking and N. M. Wereley, "Analysis of nonlinear elastic behavior in miniature pneumatic artificial muscles," *Smart Materials and Structures*, vol. 22, no. 1, p. 014016, 2012, doi: 10.1088/0964-1726/22/1/014016.

[58] B. Tondu, "Static Modeling of Pneumatic Artificial Muscle Actuator," in *2022 IEEE 5th International Conference on Soft Robotics (RoboSoft)*, pp. 364-369, 2022, doi: 10.1109/RoboSoft54090.2022.9762146.

[59] E. Ball and E. Garcia, "Effects of bladder geometry in pneumatic artificial muscles," *Journal of Medical Devices*, vol. 10, no. 4, 2016, doi: 10.1115/1.4033325.

[60] M. A. Al-Ibadi, F. K. Al-Assfor, and A. Al-Ibadi, "An Automatic Self Shape-Shifting Soft Mobile Robot (A4SMR)," *Robotics*, vol. 11, no. 6, p. 118, 2022, doi: 10.3390/robotics11060118.

[61] A. D. D. R. Carvalho, N. Karanth, and V. Desai, "Design and characterization of a pneumatic muscle actuator with novel end-fittings for medical assistive applications," *Sensors and Actuators A: Physical*, vol. 331, p. 112877, 2021, doi: 10.1016/j.sna.2021.112877.

[62] S. Koizumi, S. Kurumaya, H. Nabae, G. Endo, and K. Suzumori, "Braiding thin McKibben muscles to enhance their contracting abilities," *IEEE Robotics and Automation Letters*, vol. 3, no. 4, pp. 3240-3246, 2018, doi: 10.1109/LRA.2018.2851025.

[63] Q. Guan, J. Sun, Y. Liu, N. M. Wereley, and J. Leng, "Characterization and nonlinear models of bending extensile/contractile pneumatic artificial muscles," *Smart Materials and Structures*, vol. 30, no. 2, p. 025024, 2021, doi: 10.1088/1361-665X/abd4b0.

[64] A. Irawan, M. I. P. Azahar, and D. Pebrianti, "Interaction Motion Control on Tri-finger Pneumatic Grasper using Variable Convergence Rate Prescribed Performance Impedance Control with Pressure-based Force Estimator," *Journal of Robotics and Control (JRC)*, vol. 3, no. 5, 2022, doi: 10.18196/jrc.v3i5.16316.

[65] E. Harsono, J. Yang, S. Bhattacharya, and H. Yu, "Design and analysis of a novel hybrid-driven continuum robot with variable stiffness," *Mechanism and Machine Theory*, vol. 177, p. 105067, 2022, doi: 10.1016/j.mechmachtheory.2022.105067.

[66] L. Kotkas, N. Zhurkin, A. Donskoy, and A. Zharkovskij, "Design and Mathematical Modeling of a Pneumatic Artificial Muscle-Actuated

System for Industrial Manipulators," *Machines*, vol. 10, no. 10, p. 885, 2022, doi: 10.3390/machines10100885.

[67] H. Al-Mosawi, A. Al-Ibadi, and T. Abdalla, "A Comprehensive Comparison of Different Control Strategies to Adjust the Length of the Soft Contractor Pneumatic Muscle Actuator," *Iraqi J. Electr. Electron. Eng.*, vol. 18, no. 2, pp. 101-109, 2022, doi: 10.37917/ijeee.18.2.13.

[68] J. Sárosi, I. Biro, J. Nemeth, and L. Cveticanin, "Dynamic modeling of a pneumatic muscle actuator with two-direction motion," *Mechanism and Machine Theory*, vol. 85, pp. 25-34, 2015, doi: 10.1016/j.mechmachtheory.2014.11.006.

[69] S. Xie, H. Liu, and Y. Wang, "A method for the length-pressure hysteresis modeling of pneumatic artificial muscles," *Science China Technological Sciences*, vol. 63, no. 5, pp. 829-837, 2020, doi: 10.1007/s11431-019-9554-y.

[70] S. Ghosh, D. Kumar, and S. Roy, "Static Modeling of Braided Pneumatic Muscle Actuator: An Amended Force Model," 2021, doi: 10.21203/rs.3.rs-572133/v1.

[71] A. Stilli, L. Grattarola, H. Feldmann, H. A. Wurdemann, and K. Althoefer, "Variable Stiffness Link (VSL): Toward inherently safe robotic manipulators," in *2017 IEEE International Conference on Robotics and Automation (ICRA)*, pp. 4971-4976, 2017, doi: 10.1109/ICRA.2017.7989578.

[72] A. Stilli, H. A. Wurdemann, and K. Althoefer, "A novel concept for safe, stiffness-controllable robot links," *Soft robotics*, vol. 4, no. 1, pp. 16-22, 2017, doi: 10.1089/soro.2016.0015.

[73] I. Onda, K. Tadakuma, M. Watanabe, K. Abe, T. Watanabe, M. Konyo, and S. Tadokoro, "Highly Articulated Tube Mechanism With Variable Stiffness and Shape Restoration Using a Pneumatic Actuator," *IEEE Robotics and Automation Letters*, vol. 7, no. 2, pp. 3664-3671, 2022, doi: 10.1109/LRA.2022.3147246.

[74] M. Doumit and J. Leclair, "Development and testing of stiffness model for pneumatic artificial muscle," *International Journal of Mechanical Sciences*, vol. 120, pp. 30-41, 2017, doi: 10.1016/j.ijmecsci.2016.11.015.

[75] Y. Shan, M. Philen, A. Lotfi, S. Li, C. E. Bakis, C. D. Rahn, and K.-W. Wang, "Variable stiffness structures utilizing fluidic flexible matrix composites," *Journal of Intelligent Material Systems and Structures*, vol. 20, no. 4, pp. 443-456, 2009, doi: 10.1177/1045389X08095270.

[76] J. López-Martínez, J. L. Blanco-Claraco, D. García-Vallejo, and A. Giménez-Fernández, "Design and analysis of a flexible linkage for robot safe operation in collaborative scenarios," *Mechanism and Machine Theory*, vol. 92, pp. 1-16, 2015, doi: 10.1016/j.mechmachtheory.2015.04.018.

[77] X. Zhang, W. Ge, H. Fu, R. Chen, T. Luo, and M. Hashimoto, "A human-robot interaction based coordination control method for assistive walking devices and an assessment of its stability," *Mathematical Problems in Engineering*, vol. 2018, 2018, doi: 10.1155/2018/9279627.

[78] G. Elena, "Novel design of a soft lightweight pneumatic continuum robot arm with decoupled variable stiffness and positioning," *Soft robotics*, vol. 5, no. 1, 2018, doi: 10.1089/soro.2016.0066.

[79] L. A. Al Abeach, S. Nefti-Meziani, and S. Davis, "Design of a variable stiffness soft dexterous gripper," *Soft robotics*, vol. 4, no. 3, pp. 274-284, 2017, doi: 10.1089/soro.2016.0044.

[80] J. Mi, G. Huang, and J. Yu, "Characterization and Joint Control Study of Pneumatic Artificial Muscles," *Applied Sciences*, vol. 13, no. 2, p. 1075, 2023, doi: 10.3390/app13021075.

[81] H. Al-Fahaam, S. Davis, and S. Nefti-Meziani, "The design and mathematical modelling of novel extensor bending pneumatic artificial muscles (EBPAMs) for soft exoskeletons," *Robotics and Autonomous Systems*, vol. 99, pp. 63-74, 2018, doi: 10.1016/j.robot.2017.10.010.

[82] N. Tsagarakis and D. G. Caldwell, "Improved modelling and assessment of pneumatic muscle actuators," *Proceedings 2000 ICRA. Millennium Conference. IEEE International Conference on Robotics and Automation. Symposia Proceedings (Cat. No.00CH37065)*, vol. 4, pp. 3641-3646, 2000, doi: 10.1109/ROBOT.2000.845299.